THE GEOLOGICAL SOCIETY OF AMERICA®

Large-scale basement mobilization endows the giant Carlin-type gold mineralization in the Youjiang Basin, South China: Insights from mercury isotopes

Wei Gao[1], Ruizhong Hu[1,2,†], Xueyun Wang[1,2], Runsheng Yin[1], Xianwu Bi[1], Zhuojun Xie[1], Shanling Fu[1], and Jun Yan[1]

[1]*State Key Laboratory of Ore Deposit Geochemistry, Institute of Geochemistry, Chinese Academy of Sciences, Guiyang 550081, China*
[2]*College of Earth and Planetary Sciences, University of Chinese Academy of Sciences, Beijing 100049, China*

ABSTRACT

The metal source and genesis of hydrothermal mercury-rich gold metallogenic systems occurring far away from active continental margins remain puzzling. The Youjiang Basin of South China, where exists numerous Carlin-type gold deposits and some synmineralization hidden intrusions, is a natural laboratory to address this issue due to it was up to 1000 km inward from the active continental margins of South China when mineralization. Here, we use mass-independent fractionation of mercury isotope ratios (reported as Δ^{199}Hg), which is predominantly generated during Hg photochemical reactions on Earth's surface and has superiority of isotopic inheritance during hydrothermal processes, to address the metal source of the Youjiang Carlin-type gold deposits. Ore-associated sulfides from seven representative deposits display negative to near-zero Δ^{199}Hg values (–0.29‰ to 0.04‰), which fall in between that of the regional Precambrian basement rocks (–0.21‰ to 0.06‰) and deep magmatic-hydrothermal systems (~0‰), suggesting a binary mixing of Hg from these two sources. An isotope mixing model and mass balance calculations demonstrate that ~1000 km^3 of the basement rocks, which contributed to 86% of Hg budget, were leached and remobilized by magmatic-hydrothermal fluids and deep-circulating crustal fluids to endow the gold reserves of these deposits. Given that traditional S, Pb, C, and O isotopic data yielded indirect and ambiguous constraints on metal source due to their complex evolution processes and isotope fractionation during the fluids ascended. Our results, therefore, highlight the great advantage of using Hg isotope as a new tracer to understand metal sources of hydrothermal deposits.

†Corresponding author: huruizhong@mail.gyig.ac.cn.

INTRODUCTION

Hydrothermal gold (Au) metallogenesis occurring at active continental margins, represented by porphyry and epithermal Au deposits, has been well explained by plate subduction-related processes (Richards, 2009; Sillitoe, 2010; Wilkinson, 2013). Ore-forming materials in these deposits are suggested to be derived from the underlying mantle wedge and/or subcontinental lithospheric mantle that have been metasomatized by subducted slab- and sediments-derived fluids (Richards, 2009; Sillitoe, 2010; Griffin et al., 2013; Wilkinson, 2013; Groves et al., 2020). In contrast, the genesis and metal source of hydrothermal Au deposits formed far away from active continental margins, like the world's second-largest Carlin-type Au province in the Youjiang Basin, South China, remain highly enigmatic (Pirajno et al., 2009; Hu et al., 2017, 2020). Suggested candidates accounting for the anomalous amount of Au in this province include hydrothermal leaching of supracrustal sedimentary rocks (Gu et al., 2012), metamorphic devolatilization of the Precambrian basements (Su et al., 2009), remobilization of deep mantle-derived fertile juvenile cumulates (Zhu et al., 2020), fluid exsolution of deep magmatic-hydrothermal systems (Xie et al., 2018a; Jin et al., 2020), or dehydration and melting of subducted oceanic crust (Jin et al., 2021). Traditional stable isotopes (C, H, O, S, and noble gases) provide important constraints on the sources and evolution processes of volatile components and hydrothermal fluids (LaFlamme et al., 2018; Yan et al., 2018; Wu et al., 2019; Jin et al., 2021; Long et al., 2022). However, they cannot represent the metal sources, due to their different geochemical behavior from Au and isotope fractionation during mineralization. As such, a robust tracer that can directly fingerprint the source reservoirs of metal is urgent.

Mercury (Hg) is an important associated metal with Au in hydrothermal gold deposits (Deng et al., 2021), particular for Carlin-type Au deposits where Hg and Au are cogenetic (Cline et al., 2005; Xie et al., 2018a). Mercury isotopes undergo both mass-dependent fractionation (MDF, reported as δ^{202}Hg) and mass-independent fractionation (MIF, reported as Δ^{199}Hg). MDF-Hg occurs during various hydrothermal processes (e.g., boiling, volatilization, and mineral precipitation; Smith et al., 2005, 2008; Tang et al., 2017; Fu et al., 2020a), and therefore cannot provide direct source constraints. MIF-Hg, however, occurs mainly during photochemical reactions of Hg(II) on Earth's surface with little interference from other processes (Blum et al., 2014). Hg(II) photoreduction results in specific negative and positive Δ^{199}Hg compositions in terrestrial (e.g., soil) and oceanic (e.g., seawater and marine sediments) reservoirs, respectively (Blum et al., 2014), distinguishing them from the primitive mantle (Δ^{199}Hg ~0‰, Sherman et al., 2009; Moynier et al., 2021). Sedimentation, metamorphism, magmatism, and hydrothermal processes are not known to induce MIF-Hg (Thibodeau et al., 2016; Grasby et al., 2019; Moynier et al., 2021; Deng et al., 2021, 2022a, 2022b, 2022c; Yin et al., 2022). Therefore, Δ^{199}Hg signatures are indelibly inherited from source regions during mineralization processes. This preservation makes Δ^{199}Hg a diagnostic tracer of metal source in hydrothermal deposits, which is highlighted by the recent identification of positive Δ^{199}Hg values (up to 0.6‰) in igneous rocks and epithermal Au deposits at active continental margins worldwide, suggesting the recycling of Hg from oceanic reservoirs into deep mantle and arc

GSA Bulletin; November/December 2023; v. 135; no. 11/12; p. 3163–3172; https://doi.org/10.1130/B36636.1; 6 figures; 2 tables; 1 supplemental file.
Published online 16 March 2023

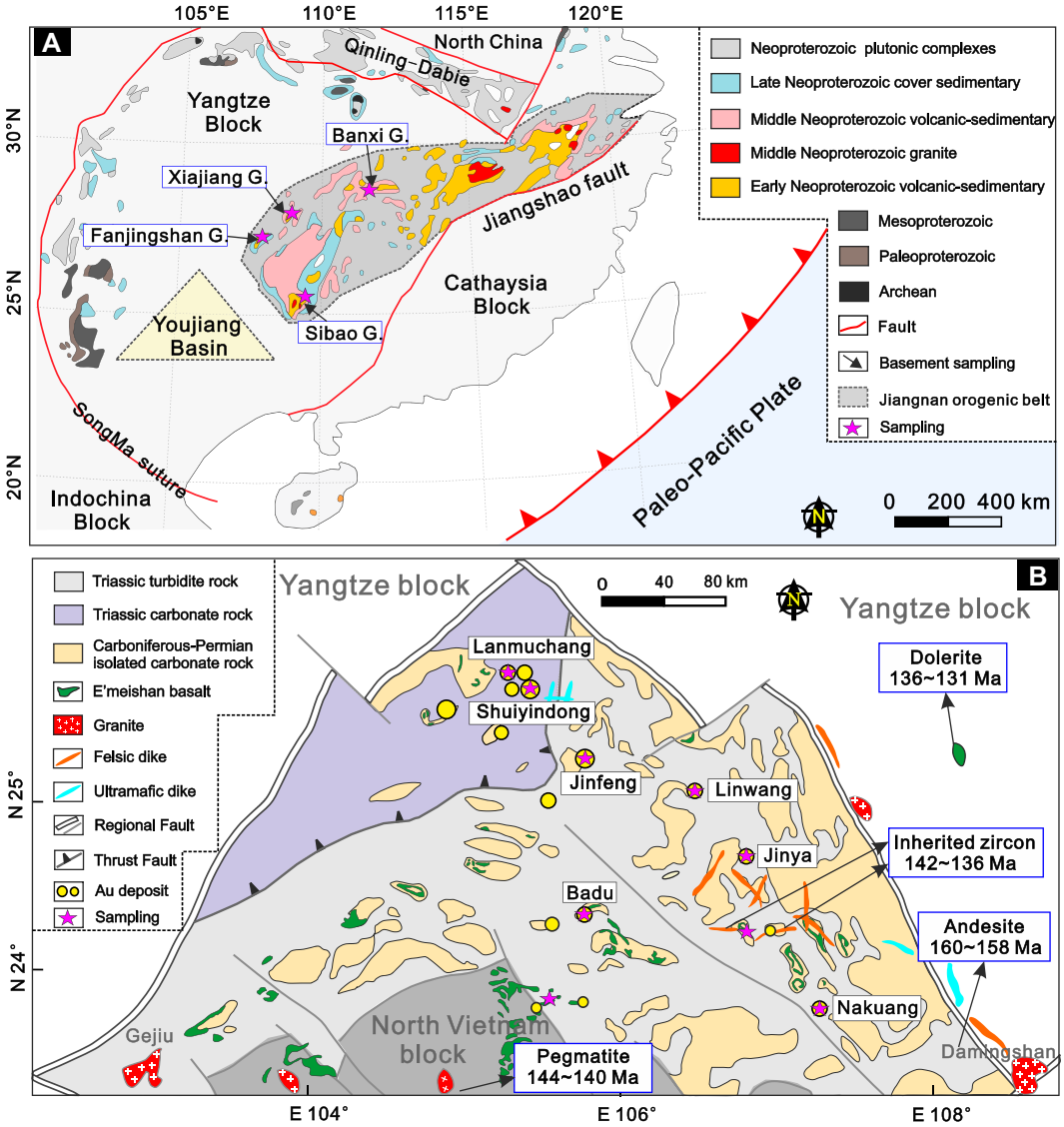

Figure 1. (A) Geological map of South China showing the distribution of the Precambrian basement rocks in the Yangtze block (modified from Zhao and Cawood, 2012). (B) Geologic map of the Youjiang Basin showing the investigated Carlin-type Au deposits in this study (modified from Gao et al., 2021). The ages of magmatic rocks are from Li et al. (2013), Zhu et al. (2016), Gan et al. (2020), and Su et al. (2021).

magma-related hydrothermal systems via plate subduction (Deng et al., 2021; Yin et al., 2022).

The Youjiang Basin is the world's second-largest Carlin-type Au province with gold reserves of over 1000 t (Hu et al., 2020). Given their distinct metallogenic setting from the epithermal Au deposits at active continental margins and their unclear metal sources (Hu et al., 2017), a systematic Hg isotope study can provide new insight into the metal source and metallogenic processes of Carlin-type Au deposits in the Youjiang Basin. We hereby present systematic Hg isotope data on seven representative Carlin-type Au deposits and potential source rocks to address their metal sources and genesis.

GEOLOGICAL BACKGROUND

The South China Block, separated from the Indochina and North China blocks by the Triassic SongMa Suture and Qingling-Dabie Orogen, respectively, comprises the Yangtze and Cathaysia blocks that were welded together along the Jiangnan Orogen at ca. 830 Ma (Fig. 1A; Zhao and Cawood, 2012). The Youjiang Basin is adjacent to the southwest of the Jiangnan Orogen, where the Precambrian basement is dominated by Neoproterozoic low-grade metamorphic volcanic-sedimentary rocks (Fig. 1B). In detail, the early Neoproterozoic Fanjinshan Group and its equivalents mainly consist of sandstone, siltstone, slate, and phyllite, which were deposited within a retro-arc foreland basin and derived from terrigenous weathering of continental crust (Fig. 2; Wei et al., 2018). The middle Neoproterozoic Banxi Group and its equivalents mainly comprise terrigenous sandstone, slate, conglomerate, and pelite deposited in intracontinental rifting basin (Fig. 2; Yao et al., 2019). Overlying strata consist of the late Neoproterozoic unmetamorphosed clastic rocks and tillite, and the Cambrian to Middle Triassic marine sedimentary covers (Hu et al., 2017).

The Carlin-type Au deposits in the Youjiang Basin are clustered along regional NE- and NW-striking faults and are mainly hosted within reactive dolomitic units of the Late Permian and Middle Triassic marine strata (Fig. 1B; Hu et al., 2017). Minor deposits occur in the Cambrian to Carbonaceous strata and Indosinian dolerite (Su et al., 2018; Gao et al., 2021). The Au mineralization is stratigraphically or structurally controlled and displays decarbonation, silicification, argillization, and sulfidation alterations (Hu et al., 2017; Su et al., 2018). Gold predominantly occurs as "invisible" Au in the lattices of arsenian pyrite or arsenopyrite that are invariably enriched in As, Sb, Hg, and Tl (Su et al., 2018; Xie et al., 2018a). Other ore minerals include stibnite,

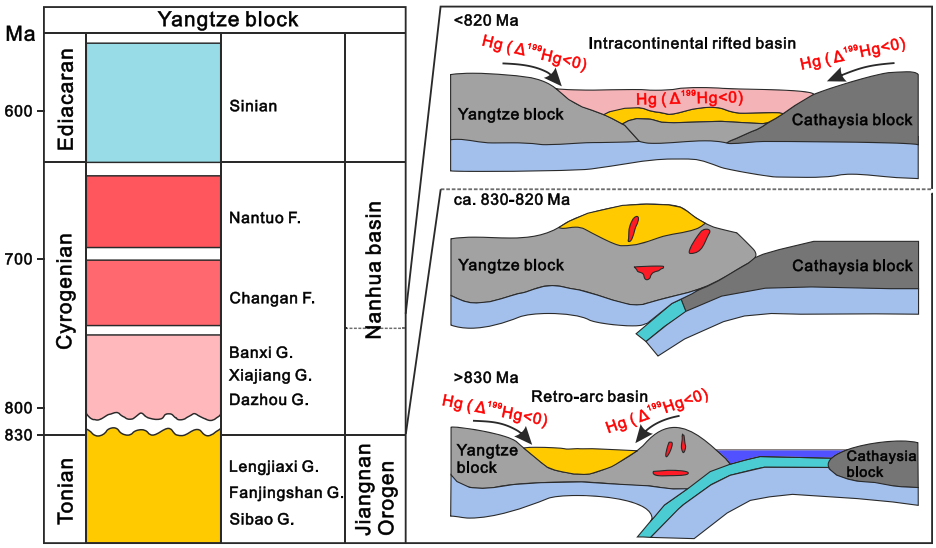

Figure 2. Time space plot showing the Neoproterozoic sedimentary sequences of the Yangtze block and tectonic evolution model of the Fanjingshan and Banxi groups (G.) of South China (modified from Wei et al., 2018; Yao et al., 2019). F.—Formation.

realgar, orpiment, and cinnabar (Hu et al., 2017). Ore-forming fluids have low temperature (180–240 °C), low salinity (<6.0 wt% NaCl equiv.), and moderately acidic to neutral pH (Su et al., 2009; Gu et al., 2012; Xie et al., 2018b). These characteristics are comparable with those of typical Carlin-type Au deposits in Nevada, USA (Hu et al., 2017; Wang and Groves, 2018; Xie et al., 2018b; Su et al., 2018; Gao et al., 2021).

Recently, reliable dating suggests that these deposits mainly formed at ca. 150–130 Ma (Su et al., 2018; Chen et al., 2019; Gao et al., 2021), with minor occurring at ca. 220–200 Ma (Pi et al., 2017). Here we focus on the main episode of Au mineralization at ca. 150–130 Ma, when Paleo-plate reconstruction and geological and geophysical evidences suggest that the Youjiang Basin was far away (up to 1000 km) from the active continental margins of the South China Block (Fig. 1A; Maruyama et al., 1997; Huang and Zhao, 2006; Seton et al., 2012; Hu et al., 2017). Li and Li (2007) and Mao et al. (2021) proposed that the vast inland of the South China Block at that time was in lithosphere extensional setting due to asthenosphere upwelling related to rollback of the Paleo-Pacific subducted slab. Some igneous rocks broadly coeval with Carlin-type Au mineralization are recently reported within and around the Youjiang Basin (Fig. 1B; Li et al., 2013; Zhu et al., 2016; Gan et al., 2020; Su et al., 2021). Geochemical data suggest that these magmatic rocks formed in a within-plate setting (Gan et al., 2020; Su et al., 2021). Aeromagnetic anomalies implied the presence of broad hidden felsic magmatic intrusions beneath the basin (Su et al., 2018). In addition, mafic rocks related to the Permian E'meishan plume are locally exposed within the basin.

SAMPLING

A total of 101 mineralized samples from seven Carlin-type Au deposits, namely Shuiyindong, Lanmuchang, Jinfeng, Linwang, Jinya, Nakuang, and Badu deposits (Fig. 1B) throughout the Youjiang Basin were collected in this study. These deposits are representative of various styles of Au mineralization with different host rocks (bioclastic limestone, siliciclastic rock, and dolerite), mineralization styles (strata-bound, fault-bound, and compound), ore mineralogy, and size (Table 1). For minimizing the effect of Hg contamination

TABLE 1. MAJOR GEOLOGICAL FEATURES OF THE CARLIN-TYPE Au DEPOSITS IN THIS STUDY

Deposit	Reserves (t)	Grade (g/t)	Styles	Host rocks	Hosting strata	Alterations	Ore minerals	References
Shuiyindong (Au)	265	5	Strata-bound	Argillite intercalated with bioclastic limestone	Longtan Formation of Upper Permian (P_3l)	Decarbonation, silicification, sulfidation, argillization	Arsenian pyrite, minor arsenopyrite, stibnite, realgar, orpiment	Su et al. (2009); Xie et al. (2018a)
Jinfeng (Au)	109	3.8	Fault-bound	Dolomitic carbonaceous siltstone	Xuman and Bianyang formations of Middle Triassic (T_2xm, T_2by)	Decarbonation, silicification, sulfidation, argillization	Arsenian pyrite, minor arsenopyrite, stibnite, realgar, orpiment	Chen et al. (2011); Xie et al. (2018a)
Linwang (Au)	>20	4	Compound	Dolomitic carbonaceous siltstone and mudstone	Baifeng Formation of Middle Triassic (T_2bf)	Decarbonation, silicification, sulfidation, argillization	Arsenian pyrite, minor arsenopyrite, stibnite, realgar, orpiment	Chen (2017, personal commun.); Gao et al. (2021)
Jinya (Au)	35	3	Fault-bound	Dolomitic carbonaceous siltstone and mudstone	Baifeng Formation of Middle Triassic (T_2bf)	Decarbonation, silicification, sulfidation, argillization	Arsenopyrite, arsenian pyrite, stibnite, realgar, orpiment	Chen et al. (2015); China Geology Survey (2015)
Nakuang (Au)	10	2	Fault-bound	Dolomitic carbonaceous siltstone and mudstone	Baifeng Formation of Middle Triassic (T_2bf)	Decarbonation, silicification, sulfidation, argillization	Arsenopyrite, arsenian pyrite, stibnite, realgar, orpiment	Gao et al. (2021)
Badu (Au)	35	2	Fault-bound	Dolerite/carbonaceous mudstone	Dolerite/Yujiang Formation of Lower Devonian (D_{1y})	Carbonation, decarbonation, sulfidation, argillization	Arsenian pyrite, arsenopyrite, stibnite, realgar, orpiment	Gao et al. (2021)
Lanmuchang (Hg-Au)	Hg:4863 Au: ?	0.19% Au: ?	Strata-bound	Argillite, bioclastic limestone, and siltstone	Longtan Formation of Upper Permian (P_3l)	Silicification, sulfidation, kaolinization, baritization	Cinnabar, lorandite, pyrite, realgar, orpiment, stibnite	Hu et al. (2017)

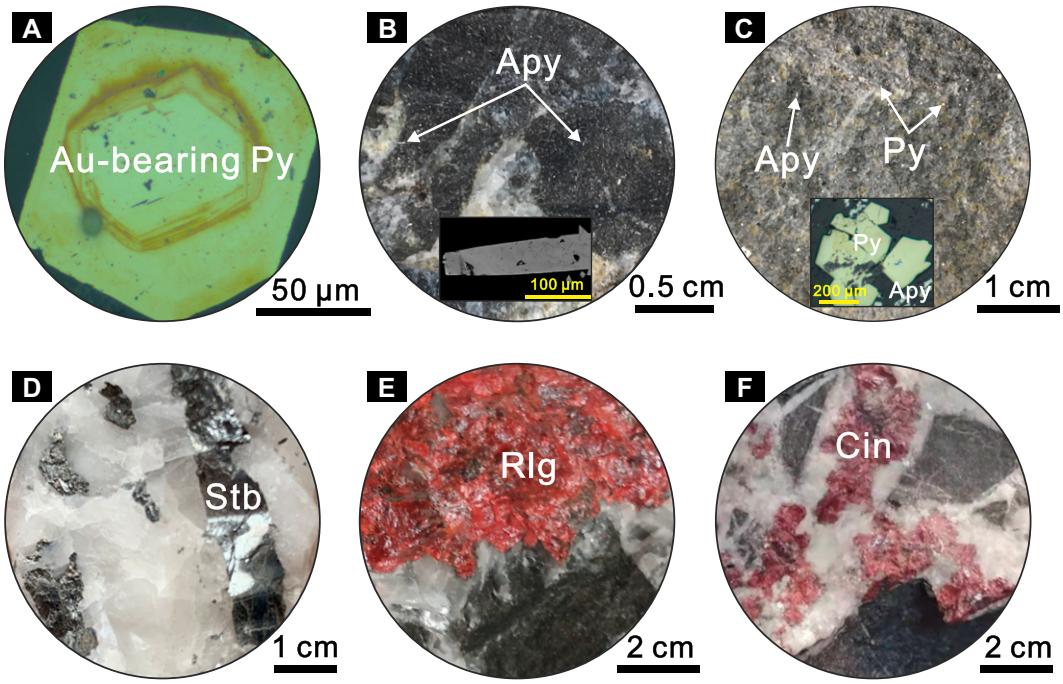

Figure 3. Photomicrographs and photographs showing mineralogy and textures of ore-associated minerals of the Carlin-type Au deposits in the Youjiang Basin of South China. (A) Au-bearing pyrite (Py) from Shuiyindong. (B) Disseminated Au-bearing arsenopyrite (Apy) from Jinya. Illustration shows the homogeneous texture of Au-bearing arsenopyrite. (C) Disseminated pyrite and arsenopyrite in the dolerite-hosted Badu deposit. Illustration shows pyrite intergrown with arsenopyrite. (D–F) Paragenetically late stibnite (Stb), realgar (Rlg), and cinnabar (Cin), respectively.

from sedimentary hosts, ore-associated pyrite (n = 47), arsenopyrite (n = 13), stibnite (n = 9), realgar (n = 5), orpiment (n = 2), and cinnabar (n = 25) were separated for further analysis. Arsenian pyrite is the predominant Au-bearing sulfide in the Shuiyindong, Jinfeng, and Linwang deposits (Fig. 3A). However, arsenopyrite is preponderant in the Jinya and Nakuang deposits (Fig. 3B). These sulfides occur as dense disseminations in strongly decarbonated and silicified bioclastic limestone or calcareous siltstone. High-contrast backscattered electron imaging shows that Au-bearing pyrite grains are characterized by core-rim texture (Figs. 3A and 4A). In contrast, Au-bearing arsenopyrite grains display homogeneous appearance (Fig. 3B). In the dolerite-hosted Badu deposit, disseminated pyrite and arsenopyrite constitute the major Au-bearing sulfides with variable relative proportions in different orebodies (Fig. 3C). Our previous study has suggested that the pyrite and arsenopyrite of Badu are hydrothermal origin and related to Au mineralization (Gao et al., 2021). In all deposits, realgar, orpiment, stibnite, and cinnabar occur as open-space infillings and are intergrown with euhedral quartz and/or calcite, constituting the paragenetically late sulfides (Figs. 3D–3F). These sulfides commonly display coarse-grained, euhedral, and homogeneous crystals.

Additionally, potential rocks of metal source including 16 Precambrian basement rocks and nine E'meishan plume-related mafic rocks were taken from the interior and periphery of the Youjiang Basin. Sample details are summarized in Table S1[1]. All selected samples are fresh rocks and devoid of weathering, alteration, and mineralization. Marine sedimentary covers in the Youjiang Basin were not collected in this study but have been investigated by Yin et al. (2017, 2019) and Deng et al. (2022b).

ANALYTICAL METHODS

Element Mapping of Au-Bearing Pyrite

For revealing variations in concentration of the trace elements in Au-bearing pyrite with core-rim texture, particular for Au and Hg. Representative Au-bearing pyrite grains were selected for trace element mapping using a Photon Machines Analyte G2 laser ablation system (193 nm, 4-ns Excimer laser) coupled to a PerkinElmer DRC-e inductively coupled plasma–mass spectrometer (ICP-MS) at the U.S. Geological Survey, Denver, Colorado, USA. The ablated material was transported to a modified glass mixing bulb. Mixtures of He (800 ml/min) and Ar (600 ml/min) were applied as the carrier gas to improve the efficiency of aerosol transport. The procedure follows the methods of Koenig et al. (2009). In this study, map ablations were conducted using a beam size of 8 μm, scanning speed of 2 μm/s, energy density of 4 J/cm^2, and repetition rate of 20 Hz. The protocol from Longerich et al. (1996) was used to calculate the concentration, and the ^{57}Fe was used as the internal standard for concentration calculations.

Hg Concentrations and Isotope Compositions

All treated samples were cleaned with deionized water, air-dried, and grinned to 200 mush in agate. Hg concentrations and isotopic compositions were measured at the Institute of Geochemistry, Chinese Academy of Sciences, using a DMA-80 Hg analyzer and Neptune Plus multi-collector (MC) ICP-MS, respectively.

For ore-associated sulfides, ~50 mg of each sample were digested with 2 mL aqua regia (HCl/HNO_3 = 3/1, v/v) in a water bath (95 °C) for 12 h before chemical analysis. For basement and dolerite samples, a double-stage tube furnace coupled with 40% anti aqua regia (HNO_3/

[1]Supplemental Material. Text S1: Mercury isotopic composition of terrestrial and marine reservoirs. Figure S1: Plots of δ^{202}Hg versus Δ^{199}Hg (a), and Δ^{201}Hg versus Δ^{199}Hg (b) of terrestrial and marine reservoirs. Text S2: Two endmember mixing model of mercury isotope. Table S1: Descriptions of the Precambrian basement rocks collected in this study from the periphery the Youjiang basin of South China. Table S2: THg and Hg isotopic compositions of ore-associated sulfides of the Carlin-type gold deposits in the Youjiang basin of South China. Table S3: THg and Hg isotopic compositions of Precambrian basement rocks from the periphery of the Youjiang basin, respectively. Table S4: THg and Hg isotopic compositions of the Permian E'meishan plume-related mafic rocks from the interior of the Youjiang basin, respectively. Please visit https://doi.org/10.1130/GSAB.S.21684908 to access the supplemental material, and contact editing@geosociety.org with any questions.

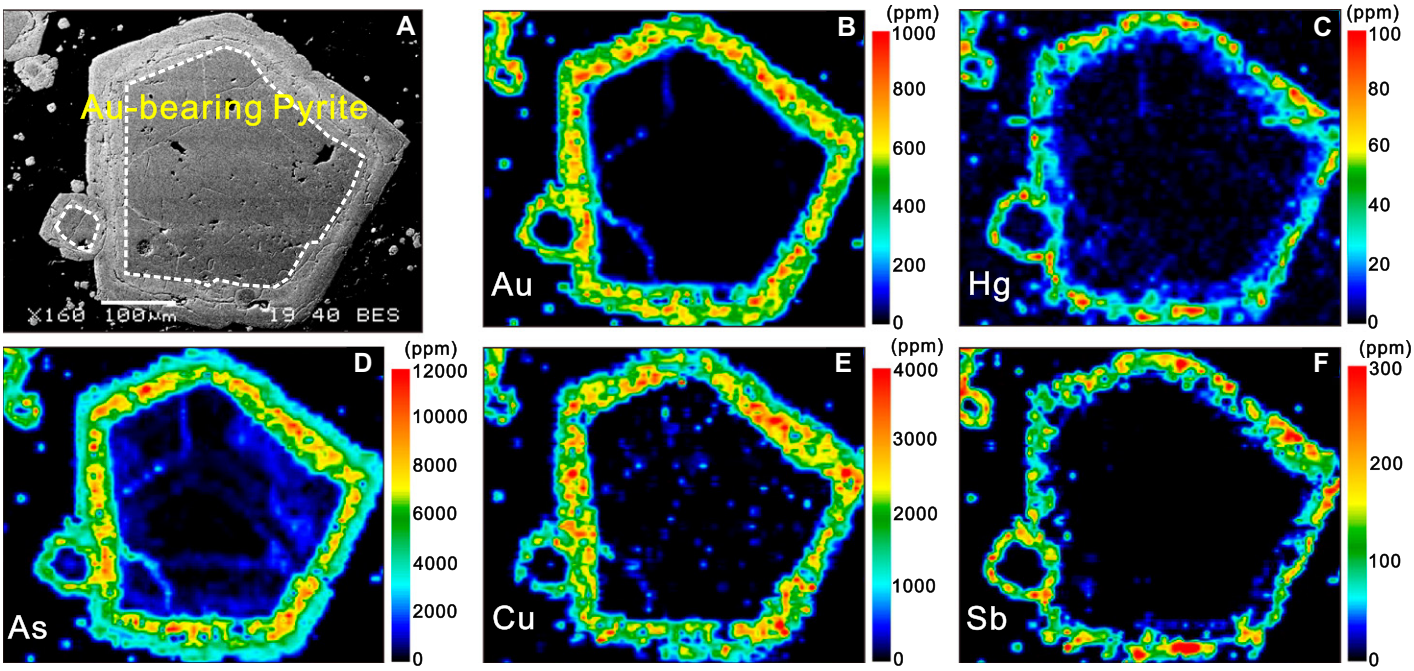

Figure 4. Backscattered electron images (A) and laser ablation–inductively coupled plasma–mass spectrometry maps of Au (B), Hg (C), As (D), Cu (E), and Sb (F) of Au-bearing pyrite from Shuiyindong deposit in the Youjiang Basin of South China, showing the correlation of these elements in pyrite core and rim.

HCl = 2/1, v/v) trapping solutions were used for Hg preconcentration, following a method by Zerkle et al. (2020). Certified reference material (GSS-4, soil) was prepared using the same process. Total Hg (THg) concentrations of the digests and preconcentrated solutions were measured by cold vapor atomic absorption spectrometry, following a method by Yin et al. (2013). The recoveries of Hg for GSS-4 are between 90% and 110%, and the relative variability of sample triplicates was <8%.

Using the THg concentrations measured above, the digests were diluted to 0.5 ng/mL Hg with 10% HCl before Hg isotope analysis using MC-ICP-MS, following a method by Yin et al. (2016). Mercury isotopic compositions were reported following the convention recommended by Blum and Bergquist (2007). Specifically, MDF-Hg is expressed in δ^{202}Hg notation in units of ‰ referenced to the NIST-3133 Hg isotope ratio standard (analyzed before and after each sample):

$$\delta^{202}\mathrm{Hg}(‰) = [(^{202}\mathrm{Hg}/^{198}\mathrm{Hg}_{\mathrm{sample}})/(^{202}\mathrm{Hg}/^{198}\mathrm{Hg}_{\mathrm{standard}}) - 1] \times 1000.$$

MIF-Hg is expressed in Δ^{xxx}Hg notation in units of parts per thousand (‰), which represents the difference between the measured δ^{xxx}Hg and the theoretically predicted δ^{xxx}Hg value:

$$\Delta^{xxx}\mathrm{Hg} \approx \delta^{xxx}\mathrm{Hg} - \delta^{202}\mathrm{Hg} \times \beta.$$

β is 0.2520 for ^{199}Hg, 0.5024 for ^{200}Hg, and 0.7520 for ^{201}Hg (Blum and Bergquist, 2007). Hg concentrations and acid matrices in the bracketing NIST-3133 solutions were matched well with the neighboring samples. Analytical uncertainty was estimated based on the replicate analyses of the NIST-3177 standard solution. The overall average and uncertainty of NIST-3177 (δ^{202}Hg: -0.50 ± 0.10‰; Δ^{199}Hg: -0.01 ± 0.06‰; Δ^{201}Hg: -0.03 ± 0.05‰; 2SD, n = 11) and GSS-4 (δ^{202}Hg: -1.78 ± 0.12‰; Δ^{199}Hg: -0.41 ± 0.06‰; Δ^{201}Hg: -0.40 ± 0.06‰; 2SD, n = 5) agree well with previous results (Blum and Bergquist, 2007; Sun et al., 2019). The larger values of standard deviation (2SD) for either NIST-3177 or GSS-4 are used to reflect analytical uncertainties for δ^{202}Hg and Δ^{199}Hg, respectively.

RESULTS

Laser Ablation (LA)-ICP-MS Mapping

The distribution of trace elements in Au-bearing pyrite with core-rim texture is displayed in Figure 4. Mapping results suggest that ore-forming elements of Au, Hg, As, Cu, and Sb are only significantly enriched in the pyrite rim. Quantitative spot analysis by Xie et al. (2018a) suggests that the pyrite rim contains up to 2800 and 1300 μg/g of Au and Hg. In contrast, these elements are extremely depleted in the pyrite core. Some cauliflower-like strings with elevated As and Au contents in the core are due to the penetration of the rim.

Hg Concentrations and Isotope Compositions

Hg concentrations and isotope compositions of ore-associated sulfides, basement rocks, and mafic rocks related to the E'meishan plume are given in Tables S2, S3, and S4, respectively. Hg concentrations of sulfides vary from 0.13 to 1300 μg/g, 10^2 to 10^7 times higher than that of the basement rocks (8–60 ng/g) and mafic rocks (0.3–2.8 ng/g). As shown in Figure 5A: (1) The mafic rocks exhibit δ^{202}Hg and Δ^{199}Hg values of −1.33‰ to −0.1‰ and 0‰–0.06‰, respectively. The Δ^{199}Hg values are consistent with previous estimates on the primitive mantle (Δ^{199}Hg ~0‰, Moynier et al., 2021). (2) The sulfides yielded δ^{202}Hg and Δ^{199}Hg values of −1.61‰ to 1.21‰ and −0.29‰ to 0.04‰, respectively, overlapping with those of the basement rocks (δ^{202}Hg = −1.25 to 1.75‰, Δ^{199}Hg = −0.21‰ to 0.06‰); The overall variation in Δ^{199}Hg is about six times the analytical uncertainty (0.06‰), clearly demonstrating the pronounced MIF-Hg signals in the Youjiang Carlin-type Au deposits. (3) Previous results from bulk ore samples in the Shuiyindong deposit (δ^{202}Hg = −1.19‰ to 0.79‰, Δ^{199}Hg = −0.14‰ to 0.02‰, Yin et al., 2019)

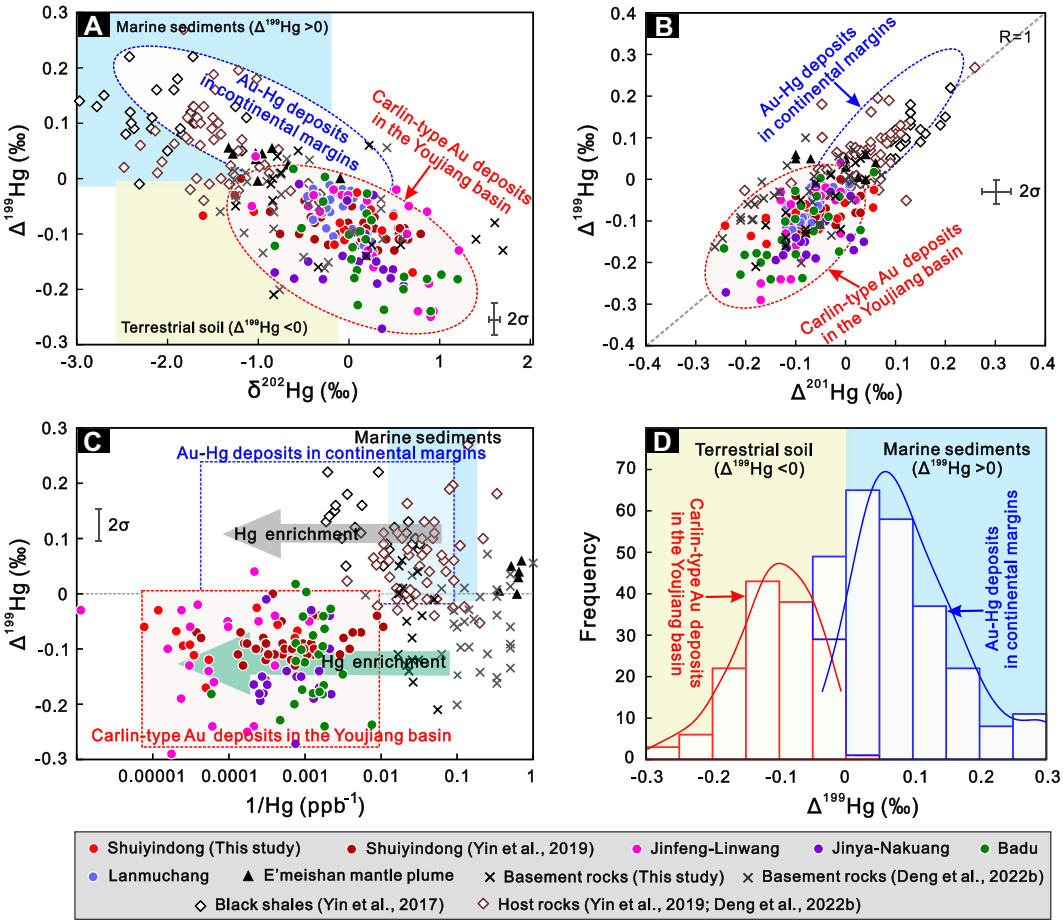

Figure 5. Plots of δ^{202}Hg versus Δ^{199}Hg (A), Δ^{201}Hg versus Δ^{199}Hg (B), 1/Hg versus Δ^{199}Hg (C), and frequency of Δ^{199}Hg (D) for the representative Carlin-type Au deposits and potential metal sources in the Youjiang Basin of South China. The data defining the areas of terrestrial and marine reservoirs and hydrothermal Au-Hg deposits at active continental margins are from Deng et al. (2021, and references therein).

are integrated into our data set. Together, a positive correlation between Δ^{199}Hg and Δ^{201}Hg, with Δ^{199}Hg/Δ^{201}Hg of ~1.0, can be observed (Fig. 5B).

Clearly, the mostly negative Δ^{199}Hg values in the Youjiang Carlin-type Au deposits are strikingly different from the positive Δ^{199}Hg values reported for the Phanerozoic sedimentary successions surrounding Au mineralization within and adjacent to the Youjiang Basin (Fig. 5C; Yin et al., 2017, 2019) and epithermal Au-Hg deposits at active continental margins worldwide (Fig. 5D; Deng et al., 2021, and references therein).

DISCUSSION

Hg Isotope of Sulfides as a Tracer of Au Source

The Au-bearing pyrite grains of the sedimentary-hosted Carlin-type Au deposits in the Youjiang Basin are characterized by core-rim textures. Previous studies suggest that the rims are related to Au mineralization, while the cores formed during diagenesis or early hydrothermal events (Su et al., 2009; Xie et al., 2018a, 2018b; Gao et al., 2021). The LA-ICP-MS mapping results clearly reveal Hg significantly enriched in the Au-bearing rims. This suggests that Hg was added together with Au by ore-forming fluids, and therefore pre-ore pyrite cores have a limited effect on Hg concentrations and isotope compositions of pyrite. This is supported by the consistency of Δ^{199}Hg values between pyrite and other sulfides with homogenous textures (arsenopyrite, stibnite, and cinnabar). The consistent correlation between Au and Hg in pyrite suggests that they are a couple of cogenetic metals and therefore may share the same source in a Carlin-type Au mineralization system (Hofstra and Cline, 2000; Hu et al., 2002; Cline et al., 2005).

Precambrian Basement as a Major Source of Hg in the Studied Au Deposits

Compared to the marine sedimentary covers and mafic rocks in the Youjiang Basin, the ore-associated sulfides display more positive δ^{202}Hg values. Two potential causes could interpret this: (1) MDF-Hg during Au mineralization, e.g., the loss of isotopically light Hg during Hg(0) volatilization in hydrothermal fluids (Smith et al., 2005, 2008; Fu et al., 2020a), and isotope fractionation triggered by mineral precipitation (Tang et al., 2017); (2) Hg was initially derived from a distinct ^{202}Hg-rich metal source, such as the Precambrian basement with higher δ^{202}Hg values (Fig. 5A). Given a lack of full knowledge of all hydrothermal processes that may generate MDF-Hg, to avoid misinterpretation, we believe δ^{202}Hg is not diagnostic for Hg sources and will not discuss δ^{202}Hg further in this paper.

Instead, Δ^{199}Hg provide diagnostic constraints regarding Hg source, as MIF-Hg is mainly produced by photoreduction of Hg(II) on Earth's surface, which results in reservoir-specific Δ^{199}Hg values (Blum et al., 2014). Minimal or no MIF-Hg may occur during hydrothermal processes, e.g., leaching, mobilization, and minerals precipitation (Pribil et al., 2020; Fu et al., 2021a; Deng et al., 2021). The superiorities of isotopic inheritance and preservation of MIF-Hg makes Δ^{199}Hg an indelible tracer of metal source in mineralization systems (Deng et al., 2021, 2022b). Most of the ore-associated sulfides of Carlin-type Au deposits in the Youjiang Basin display negative Δ^{199}Hg values with Δ^{199}Hg/Δ^{201}Hg ratios of ~1.0 (Fig. 5B), which are consistent with that observed during aqueous Hg(II)

photoreduction on Earth's surface (Bergquist and Blum, 2007), suggesting that Hg in these samples was dominantly derived from recycled surface reservoirs.

The negative Δ^{199}Hg values of ore-associated sulfides are distinct from the positive Δ^{199}Hg signals of black shales and country rocks surrounding gold mineralization (Fig. 5C; Yin et al., 2017, 2019; Deng et al., 2022b), precluding sedimentary covers as the primary sources of Hg in the Youjiang Carlin-type Au deposits. Similarly, the negative Δ^{199}Hg values also are distinct from that of epithermal Au-Hg deposits at continental plate margins worldwide, which display positive Δ^{199}Hg values (0‰–0.4‰) inherited from recycled seawater and marine sediments via slab subduction (Deng et al., 2021). Therefore, we concluded that the Youjiang Carlin-type Au deposits may not be genetically related to dehydration, metasomatism, and melting of subducted slab and sediments.

The Precambrian basement rocks investigated in this study mainly display negative Δ^{199}Hg signals (−0.21‰ to 0.06‰), due to their littoral and near-coastal deposition environment (Wei et al., 2018; Yao et al., 2019), which received Hg through terrestrial soil runoff (Fig. 2; Yin et al., 2015). Therefore, the consistency in negative Δ^{199}Hg values between ore-associated sulfides and Precambrian basement rocks may reasonably suggest that significant portions of Hg and metals in the Youjiang Carlin-type Au deposits were derived from the basement (Hu et al., 2020; Deng et al., 2022b). This hypothesis aligns well with the: (1) highly radiogenic Sr and Pb isotopes of ore sulfides, indicating that ore fluids have experienced interaction with the basement rocks (Ma et al., 2003); (2) CO_2-rich fluid inclusions and O-H isotopic data of ore-stage quartz, suggestive of deep crust-derived origin for the dominant ore fluids (Su et al., 2009, 2018); (3) elevated Au, As, Sb, Cu, and Hg contents (e.g., 4.0 ng/g of Au and 59.5 ng/g of Hg) in the basement rocks (Ma et al., 2002). These elements are invariably enriched in ore-associated pyrite (Fig. 4), suggesting basement rocks as a fertile source for the Youjiang Carlin-type Au deposits.

Magmatic-Hydrothermal Contribution

Besides those showing strikingly negative values, some ore-associated sulfides yielded near-zero Δ^{199}Hg values and different deposits show different extents of MIF-Hg, suggesting mixing of an additional Hg source. Given the near-zero Δ^{199}Hg values, the E'meishan plume-related mafic rocks and deep cumulates may be a potential source. However, this is compromised by the comparative deficiency of As, Sb, and Hg in plume-related mafic rocks (Pitcairn et al., 2015, 2021). A previous study by Yin et al. (2019) attributed the near-zero to slightly negative Δ^{199}Hg values in the Shuiyindong deposit to the contribution of deep magmatic-hydrothermal fluids with no MIF-Hg. This is supported by the presence of some synmineralization igneous rocks (Fig. 1A) and hidden intrusions within and adjacent to the Youjiang Basin (Su et al., 2018). Geochemical data from some deposits also support magmatic-hydrothermal fluids as another source of metals in the Youjiang Carlin-type Au deposits, e.g., sulfur isotopic compositions of magmatic sulfur in ore sulfides ($\delta^{34}S = 0‰–5‰$, Xie et al., 2018a), noble gas isotopic ratios of mantle He in ore-stage quartz ($^3He/^4He > 0.04$ R_A, Jin et al., 2020), and trace element ratios of magmatic vapor affinity in fluid inclusions (high B/Sr, Large et al., 2016).

Overall, we suggest that the Youjiang Carlin-type Au deposits received Hg and other metals from mixing between: (1) the Precambrian basement with negative Δ^{199}Hg values of −0.21‰ to 0.06‰, and (2) the magmatic-hydrothermal fluids with Δ^{199}Hg value of close to 0‰. Based on the Δ^{199}Hg values of ore-associated sulfides, using a binary mixing model calculated by Monte Carlo simulation (see Supplementary Text S2), we roughly estimate that the Precambrian basement rocks and magmatic-hydrothermal fluids contributed ~86% and ~14% (1SD = 14%) of the Hg to the Youjiang Carlin-type Au deposits, respectively. However, it should be noted that the relative contributions of the two sources can largely vary (Table 2), as shown by the different extents of MIF-Hg among deposits.

Metallogenic Model for the Youjiang Carlin-type Au Deposits

The contribution of metals from the Precambrian basement could be via three possible ways: metamorphic devolatilization, partial melting, or hydrothermal leaching. However, the basement rocks in the Youjiang Basin only experienced low-grade to weak metamorphism, which does not support the metamorphic devolatilization model (Pitcairn et al., 2006, 2021). The contribution of metals via partial melting of basement rocks, if any, would be limited, given that magmatic fluids released from felsic melts that formed by partial melting of basement rocks cannot simultaneously enrich Au, Sb, and Hg due to the relatively low fluid-melt partition coefficient of Sb (Fu et al., 2020b). Hydrothermal leaching and remobilization of metals from the basement rocks is possibly the mechanism to form Au-, Sb-, and Hg-rich hydrothermal fluids. Ma et al. (2002) demonstrated high mobility of Au and Hg in basement rocks during hydrothermal fluid interaction, with a leaching rate of >20%. Based on the mean Au and Hg concentrations of 2 and 50 ng/g in these basement rocks (Ma et al., 2002), assuming a rock density of 2.7 g cm^{-3}, we calculated that ~1000 km^3 of the basement mass would release the estimated Au reserves of ~1000 t in the Youjiang province.

Collectively, we develop a metallogenic model for the Youjiang Carlin-type Au deposits (Fig. 6). During the Neoproterozoic, terrigenous weathering detritus formed the basement rocks of the Yangtze block with negative Δ^{199}Hg signals (Fig. 2). Thick marine sedimentary rocks with positive Δ^{199}Hg signals deposited within the Youjiang Basin from the Sinian to Middle Triassic. Large-scale lithosphere extension due to asthenosphere upwelling during the Late Jurassic–Early Cretaceous triggered extensive magmatism and mineralization in the inland of South China (Hu et al., 2017; Mao et al., 2021). Synchronous magmatism beneath the Youjiang Basin not only released magmatic-hydrothermal fluids containing a portion of Hg with near-zero Δ^{199}Hg, but drove heated deep-circulating fluids to mobilize metals from the basement rocks (Hu et al., 2020; Deng et al.,

TABLE 2. FRACTIONAL CONTRIBUTIONS OF Hg AND METALS FROM THE BASEMENT ROCKS AND MAGMATIC-HYDROTHERMAL SYSTEM FOR THE CARLIN-TYPE GOLD DEPOSITS IN THE YOUJIANG BASIN

Deposit	f_b ($\Delta^{199}Hg_b = -0.0988 \pm 0.0376$) (%)	f_m ($\Delta^{199}Hg_m = 0.0384 \pm 0.0222$) (%)	SD (%)
Shuiyindong ($\Delta^{199}Hg_s = -0.0868 \pm 0.0320$)	76	24	15
Jinfeng-Linwang ($\Delta^{199}Hg_s = -0.1032 \pm 0.0910$)	81	19	15
Jinya-Nakuang ($\Delta^{199}Hg_s = -0.1449 \pm 0.0643$)	93	7	13
Badu ($\Delta^{199}Hg_s = -0.1243 \pm 0.0747$)	88	12	14
Mean ($\Delta^{199}Hg_s = -0.1168 \pm 0.0638$)	86	14	14

Notes: f_b and f_m—the fractional contributions of basement rocks and magmatic-hydrothermal system, respectively. $\Delta^{199}Hg_b$, $\Delta^{199}Hg_m$, and $\Delta^{199}Hg_S$—mean isotopic values of basement rocks, magmatic system, and ore-associated sulfides, respectively. SD—standard deviation.

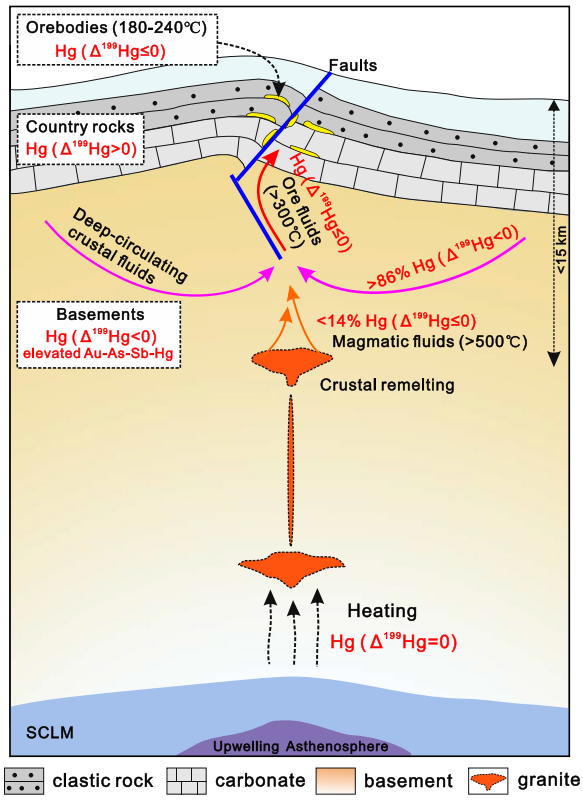

Figure 6. Metallogenic model of the Youjiang Carlin-type Au deposits of South China. SCLM—Sub-continental lithospheric mantle.

2022b), forming Au- and Hg-rich hydrothermal fluids with negative Δ^{199}Hg. The ore fluids were mixed and migrated upwards along deeply seated faults and ponded into favorable strata and structural traps (Hu et al., 2017; Su et al., 2018), generating the Youjiang Carlin-type Au deposits with negative to near-zero Δ^{199}Hg values.

CONCLUSIONS

This study observes negative to near-zero Δ^{199}Hg values in the Youjiang Carlin-type Au deposits, suggesting that the main contribution of Hg and metals was originated from the Precambrian basement. This is different from the positive to near-zero Δ^{199}Hg values observed in the epithermal Au deposits at active continental margins, which mainly receive Hg from oceanic crust and sediments via plate subduction. The negative Δ^{199}Hg values in the Youjiang Carlin-type Au deposits, perhaps, imply the Precambrian basement as a common metal source for hydrothermal Au metallogenesis occurring far away from active continental margins. Comparing the traditional S, Pb, C, and O isotopes that experienced complex evolution processes and isotope fractionation during mineralization, Hg isotope is a powerful tracer for directly constraining the metal source of hydrothermal deposits in different settings.

ACKNOWLEDGMENTS

This work was financially supported by the National Natural Science Foundation of China (grants U1812402, 41830432, 41873047). We would like to thank Yuzhou Zhuo and Jinxiang Li for their help during field work and sample analyses. Richard Goldfarb from the Colorado School of Mines and Yafei Wu from the China University of Geosciences are thanked for giving constructive suggestions that have greatly strengthened this paper. We thank two anonymous reviewers for their critical and constructive reviews, which have greatly improved the quality of the manuscript. Our thanks are extended to Science Editor Mihai N. Ducea and the Associate Editor of Geological Society of America Bulletin for handling the manuscript.

REFERENCES CITED

Bergquist, B.A., and Blum, J.D., 2007, Mass-dependent and -independent fractionation of Hg isotopes by photoreduction in aquatic systems: Science, v. 318, p. 417–420, https://doi.org/10.1126/science.1148050.

Blum, J.D., and Bergquist, B.A., 2007, Reporting of variations in the natural isotopic composition of mercury: Analytical and Bioanalytical Chemistry, v. 388, p. 353–359, https://doi.org/10.1007/s00216-007-1236-9.

Blum, J.D., Sherman, L.S., and Johnson, M.W., 2014, Mercury isotopes in earth and environmental sciences: Annual Review of Earth and Planetary Sciences, v. 42, p. 249–269, https://doi.org/10.1146/annurev-earth-050212-124107.

Chen, M.H., Mao, J.W., Bierlein, F.P., Norman, T., and Uttley, P.J., 2011, Structural features and metallogensis of the Carlin-type Jinfeng (Lannigou) gold deposit, Guizhou Province, China: Ore Geology Reviews, v. 43, p. 217–234, https://doi.org/10.1016/j.oregeorev.2011.06.009.

Chen, M.H., Mao, J.W., Li, C., Zhang, Z.Q., and Dang, Y., 2015, Re-Os isochron ages for arsenopyrite from Carlin-like gold deposits in the Yunnan-Guizhou-Guangxi "golden triangle", southwestern China: Ore Geology Reviews, v. 64, p. 316–327, https://doi.org/10.1016/j.oregeorev.2014.07.019.

Chen, M.H., Bagas, L., Liao, X., Zhang, Z.Q., and Li, Q.L., 2019, Hydrothermal apatite SIMS Th-Pb dating, Constrains on the timing of low temperature hydrothermal Au deposit in Nibao, SW China: Lithos, v. 324–325, p. 418–428, https://doi.org/10.1016/j.lithos.2018.11.018.

China Geological Survey, 2015, Discovery of large gold deposits in the Jinya deposit, Guangxi [in Chinese with English abstract]: Gold Science and Technology, v. 23, p. 54.

Cline, J.S., Hofstra, A.H., Muntean, J.L., Tosdal, R.M., and Hickey, K.A., 2005, Carlin-type gold deposits in Nevada, Critical geologic characteristics and viable models: Economic Geology 100th Anniversary Volume, p. 451–484.

Deng, C.Z., Sun, G.Y., Rong, Y.M., Sun, R.Y., Sun, D.Y., Lehmann, B., and Yin, R.S., 2021, Recycling of mercury from the atmosphere-ocean system into volcanic-arc–associated epithermal gold systems: Geology, v. 49, p. 309–313, https://doi.org/10.1130/G48132.1.

Deng, C.Z., Gou, J., Sun, D.Y., Sun, G.Y., Tian, Z.D., Lehmann, B., Moynier, F., and Yin, R.S., 2022a, Mercury isotopic composition of igneous rocks from an accretionary orogen: Implications for lithospheric recycling: Geology, v. 50, p. 1001–1006, https://doi.org/10.1130/G50131.1.

Deng, C.Z., Zhang, J.W., Hu, R.Z., Luo, K., Zhu, Y.N., and Yin, R.S., 2022b, Mercury isotope constraints on the genesis of late Mesozoic Sb deposits in South China: Science China: Earth Sciences, v. 65, p. 269–281, https://doi.org/10.1007/s11430-021-9851-x.

Deng, C.Z., Geng, H.Y., Xiao, T.T., Chen, D., Sun, G.Y., and Yin, R.S., 2022c, Mercury isotopic compositions of the Precambrian rocks and implications for tracing mercury cycling in Earth's interior: Precambrian Research, v. 373, https://doi.org/10.1016/j.precamres.2022.106646.

Fu, S.L., Hu, R.Z., Yin, R.S., Yan, J., Mi, X.F., Song, Z.C., and Sullivan, N.A., 2020a, Mercury and in situ sulfur isotopes as constraints on the metal and sulfur sources for the world's largest Sb deposit at Xikuangshan, southern China: Mineralium Deposita, v. 55, p. 1353–1364, https://doi.org/10.1007/s00126-019-00940-1.

Fu, S.L., Zajacz, A., Tsay, A., and Hu, R.Z., 2020b, Can magma degassing at depth donate the metal budget of large hydrothermal Sb deposits?: Geochimica et Cosmochimica Acta, v. 290, p. 1–15, https://doi.org/10.1016/j.gca.2020.08.029.

Gan, C.S., Wang, Y.J., Barry, T.L., Zhang, Y.Z., and Qian, X., 2020, Late Jurassic high-Mg andesites in the Youjiang Basin and their significance for the southward continuation of the Jiangnan Orogen, South China: Gondwana Research, v. 77, p. 260–273, https://doi.org/10.1016/j.gr.2019.06.018.

Gao, W., Hu, R.Z., Hofstra, A.H., Li, Q.L., Zhu, J.J., Peng, K.Q., Mu, L., Huang, Y., Ma, J.W., and Zhao, Q., 2021, U-Pb dating on hydrothermal rutile and monazite from the Badu gold deposit supports an Early Cretaceous age for Carlin-type gold mineralization in the Youjiang Basin, southwestern China: Economic Geology, v. 116, p. 1355–1385, https://doi.org/10.5382/econgeo.4824.

Grasby, S.E., Them, T.R., Chen, Z.H., Yin, R.S., and Ardakani, O.H., 2019, Mercury as a proxy for volcanic emissions in the geologic record: Earth-Science Reviews, v. 196, https://doi.org/10.1016/j.earscirev.2019.102880.

Griffin, W.L., Begg, G.C., and O'Reilly, S.Y., 2013, Continental-root control on the genesis of magmatic ore deposits: Nature Geoscience, v. 6, p. 905–910, https://doi.org/10.1038/ngeo1954.

Groves, D.I., Zhang, L., and Santosh, M., 2020, Subduction, mantle metasomatism, and gold: A dynamic and genetic conjunction: Geological Society of America Bulletin, v. 132, n. 7–8, p. 1419–1426, https://doi.org/10.1130/B35379.1.

Gu, X.X., Zhang, Y.M., Li, B.H., Dong, S.Y., Xue, C.J., and Fu, S.H., 2012, Hydrocarbon and ore-bearing basinal fluids: A possible link between gold mineralization and hydrocarbon accumulation in the Youjiang basin, South

China: Mineralium Deposita, v. 47, p. 663–682, https://doi.org/10.1007/s00126-011-0388-x.

Hofstra, A.H., and Cline, J.S., 2000, Characteristics and models for Carlin-type gold deposits: Reviews in Economic Geology, v. 13, p. 163–220.

Hu, R.Z., Su, W.C., Bi, X.W., Tu, G.Z., and Hofstra, A.H., 2002, Geology and geochemistry of Carlin-type gold deposits in China: Mineralium Deposita, v. 37, p. 378–392, https://doi.org/10.1007/s00126-001-0242-7.

Hu, R.Z., Fu, S.L., Huang, Y., Zhou, M.F., Fu, S.H., Zhao, C.H., Wang, Y.J., Bi, X.W., and Xiao, J.F., 2017, The giant South China Mesozoic low-temperature metallogenic domain: Reviews and a new geodynamic model: Journal of Asian Earth Sciences, v. 137, p. 9–34, https://doi.org/10.1016/j.jseaes.2016.10.016.

Hu, R.Z., Chen, W.T., Bi, X.W., Fu, S.L., Yin, R.S., and Xiao, J.F., 2020, Control of Precambrian basement on the formation of Mesozoic large-scale low-temperature mineralization in the Yangtze Craton [in Chinese with English abstract]: Earth Science Frontiers, v. 27, p. 137–150.

Huang, J., and Zhao, D.P., 2006, High-resolution mantle tomography of China and surrounding regions: Journal of Geophysical Research: Solid Earth, v. 111, B9, https://doi.org/10.1029/2005JB004066.

Jin, X.Y., Hofstra, A.H., Hunt, A.G., Liu, J.Z., Yang, W., and Li, J.W., 2020, Noble gases fingerprint the source and evolution of ore-forming fluids of Carlin-type gold deposits in the golden triangle, South China: Economic Geology, v. 115, p. 455–469, https://doi.org/10.5382/econgeo.4703.

Jin, X.Y., Zhao, J.X., Feng, Y.X., Hofstra, A.H., Deng, X.D., Zhao, X.F., and Li, J.W., 2021, Calcite U-Pb dating unravels the age and hydrothermal history of the Giant Shuiyindong Carlin-type gold deposit in the golden triangle, South China: Economic Geology, v. 116, p. 1253–1265, https://doi.org/10.5382/econgeo.4870.

Koenig, A.E., Rogers, R.R., and Trueman, C.N., 2009, Visualizing fossilization using laser ablation ICP-MS maps of trace elements in Late Cretaceous bones: Geology, v. 37, p. 511–514, https://doi.org/10.1130/G25551A.1.

LaFlamme, C., Sugiono, D., Thébaud, N., Caruso, S., Fiorentini, M., Selvaraja, V., Voute, F., Jeon, H., and Martin, L., 2018, Multiple sulfur isotopes monitor fluid evolution of an Archean orogenic gold deposit: Geochimica et Cosmochimica Acta, v. 222, p. 436–446, https://doi.org/10.1016/j.gca.2017.11.003.

Large, S.J.E., Bakker, E.Y.N., Weis, P., Walle, M., Ressel, M., and Heinrich, C.A., 2016, Trace elements in fluid inclusions of sediment-hosted gold deposits indicate a magmatic-hydrothermal origin of the Carlin ore trend: Geology, v. 44, p. 1015–1018, https://doi.org/10.1130/G38351.1.

Li, J.K., Wang, D.H., Li, H.Q., Chen, Z.H., and Mei, Y.P., 2013, Late Jurassic-Early Cretaceous mineralization in the Laojunshan ore concentration area, Yunnan province [in Chinese with English abstract]: Earth Science-Journal of China University of Geosciences, v. 38, p. 1023–1036.

Li, Z.X., and Li, X.H., 2007, Formation of the 1300-km-wide intracontinental orogen and postorogenic magmatic province in Mesozoic South China: A flat-slab subduction model: Geology, v. 35, p. 179–182, https://doi.org/10.1130/G23193A.1.

Long, Z.Y., Qiu, K.F., Santosh, M., Yu, H.C., Jiang, X.Y., Zou, L.Q., and Tang, D.W., 2022, Fingerprinting the metal source and cycling of the world's largest antimony deposit in Xikuangshan, China: Geological Society of America Bulletin, v. 135, no. 1–2, p. 286–294, https://doi.org/10.1130/B36377.1.

Longerich, H.P., Jackson, S.E., and Günther, D., 1996, Laser ablation inductively coupled plasma mass spectrometric transient signal data acquisition and analyze concentration calculation: Journal of Atomic Spectrometry, v. 11, p. 899–904, https://doi.org/10.1039/JA9961100899.

Ma, D.S., Pan, J.Y., Xie, Q.L., and He, J., 2002, Ore source of Sb (Au) deposits in central Hunan: I. evidences of trace element and experimental geochemistry [in Chinese with English abstract]: Mineralium Deposita, v. 21, p. 366–376.

Ma, D.S., Pan, J.Y., and Xie, Q.L., 2003, Ore source of Sb (Au) deposits in central Hunan: II. Evidences of isotopic geochemistry [in Chinese with English abstract]: Mineralium Deposita, v. 22, p. 78–87.

Mao, J.W., Liu, P., Goldfarb, R.J., Goryachev, N.A., Pirajno, F., Zheng, W., Zhou, M.F., Zhao, C., Xie, G.Q., Yuan, S.D., and Liu, M., 2021, Cretaceous large-scale metal accumulation triggered by post-subductional large-scale extension, East Asia: Ore Geology Reviews, v. 136, https://doi.org/10.1016/j.oregeorev.2021.104270.

Maruyama, S., Isozaki, Y., Kimura, G., and Terabayashi, M., 1997, Paleogeographic maps of the Japanese Islands: Plate tectonic synthesis from 750 Ma to the present: The Island Arc, v. 6, p. 121–142, https://doi.org/10.1111/j.1440-1738.1997.tb00043.x.

Moynier, F., Jackson, M., Zhang, K., Cai, H.M., Halldórsson, S.A., Pik, R., Day, J.M.D., and Chen, J.B., 2021, The mercury isotopic composition of Earth's mantle and the use of mass independently fractionated Hg to test for recycled crust: Geophysical Research Letters, v. 48, no. 17, https://doi.org/10.1029/2021GL094301.

Pi, Q.H., Hu, R.Z., Xiong, B., Li, Q.L., and Zhong, R.C., 2017, In situ SIMS U-Pb dating of hydrothermal rutile, reliable age for the Zhesang Carlin-type gold deposit in the golden triangle region, SW China: Mineralium Deposita, v. 52, p. 1179–1190, https://doi.org/10.1007/s00126-017-0715-y.

Pirajno, F., Ernst, R.E., Borisenko, A.S., Fedoseev, G., and Naumov, E.A., 2009, Intraplate magmatism in Central Asia and China and associated metallogeny: Ore Geology Reviews, v. 35, p. 114–136, https://doi.org/10.1016/j.oregeorev.2008.10.003.

Pitcairn, I.K., Teagle, D.A.H., Craw, D., Olivo, G.R., Kerrich, R., and Brewer, T.S., 2006, Sources of metals and fluids in orogenic gold deposits: Insights from the Otago and Alpine schists, New Zealand: Economic Geology, v. 101, p. 1525–1546, https://doi.org/10.2113/gsecongeo.101.8.1525.

Pitcairn, I.K., Craw, D., and Teagle, D.A., 2015, Metabasalts as sources of metals in orogenic gold deposits: Mineralium Deposita, v. 50, p. 373–390, https://doi.org/10.1007/s00126-014-0547-y.

Pitcairn, I.K., Leventis, N., Beaudoin, G., Faure, S., Guilmette, C., and Dubé, B., 2021, A metasedimentary source of gold in Archean orogenic gold deposits: Geology, v. 49, p. 862–866, https://doi.org/10.1130/G48587.1.

Pribil, M.J., Rimondi, V., Costagliola, P., Lattanzi, P., and Rutherford, D.L., 2020, Assessing mercury distribution using isotopic fractionation of mercury processes and sources adjacent to and downstream of a legacy mine district in Tuscany, Italy: Applied Geochemistry, v. 117, https://doi.org/10.1016/j.apgeochem.2020.104600.

Richards, J.P., 2009, Post-subduction porphyry Cu-Au and epithermal Au deposits: Products of remelting of subduction-modified lithosphere: Geology, v. 37, p. 247–250, https://doi.org/10.1130/G25451A.1.

Seton, M., Müller, R.D., Zahirovic, S., Gaina, C., Torsvik, T., Shephard, G., Talsma, A., Gurnis, M., Turner, M., Maus, S., and Chandler, M., 2012, Global continental and ocean basin reconstructions since 200 Ma: Earth-Science Reviews, v. 113, p. 212–270, https://doi.org/10.1016/j.earscirev.2012.03.002.

Smith, C.N., Kesler, S.E., Klaue, B., and Blum, J.D., 2005, Mercury isotope fractionation in fossil hydrothermal systems: Geology, v. 33, p. 825–828, https://doi.org/10.1130/G21863.1.

Smith, C.N., Kesler, S.E., Blum, J.D., and Rytuba, J.J., 2008, Isotope geochemistry of mercury in source rocks, mineral deposits and spring deposits of the California Coast Ranges, USA: Earth and Planetary Science Letters, v. 269, p. 399–407, https://doi.org/10.1016/j.epsl.2008.02.029.

Sherman, L.S., Blum, J.D., Nordstrom, D.K., McCleskey, R.B., Barkay, T., and Vetriani, C., 2009, Mercury isotopic composition of hydrothermal systems in the Yellowstone Plateau volcanic field and Guaymas Basin sea-floor rift: Earth and Planetary Science Letters, v. 279, p. 86–96, https://doi.org/10.1016/j.epsl.2008.12.032.

Sillitoe, R.H., 2010, Porphyry copper systems: Economic Geology, v. 105, p. 3–41, https://doi.org/10.2113/gsecongeo.105.1.3.

Su, H.M., Jiang, S.Y., Shao, J.B., Zhang, D.Y., Wu, X.K., and Huang, X.Q., 2021, New identification and significance of Early Cretaceous mafic rocks in the interior South China Block: Scientific Reports, v. 11, 11396, https://doi.org/10.1038/s41598-021-91045-1.

Su, W.C., Heinrich, C.A., Pettke, T., Zhang, X.C., Hu, R.Z., and Xia, B., 2009, Sediment-hosted gold deposits in Guizhou, China, products of wall-rock sulfidation by deep crustal fluids: Economic Geology, v. 104, p. 73–93, https://doi.org/10.2113/gsecongeo.104.1.73.

Su, W.C., Dong, W.D., Zhang, X.C., Shen, N.P., Hu, R.Z., Hofstra, A.H., and Cheng, L.Z., 2018, Chapter 5: Carlin-type gold deposits in the Dian-Qian-Gui "Golden Triangle" of southwest China, *in* Muntean, J.L., ed., Diversity of Carlin-Style Gold Deposits: Reviews in Economic Geology: Society of Economic Geologists, v. 20, p. 157–185, https://doi.org/10.5382/rev.20.05.

Sun, R.Y., Jiskra, M., Amos, H.M., Zhang, Y.X., Sunderland, E.M., and Sonke, J.E., 2019, Modeling the mercury stable isotope distribution of Earth surface reservoirs: Implications for global Hg cycling: Geochimica et Cosmochimica Acta, v. 246, p. 156–173, https://doi.org/10.1016/j.gca.2018.11.036.

Tang, Y.Y., Bi, X.W., Yin, R.S., Feng, X.B., and Hu, R.Z., 2017, Concentrations and isotopic variability of mercury in sulfide minerals from the Jinding Zn-Pb deposit, Southwest China: Ore Geology Reviews, v. 90, p. 958–969, https://doi.org/10.1016/j.oregeorev.2016.12.009.

Thibodeau, A.M., Ritterbush, K., Yager, J.A., West, A.J., Ibarra, Y., Bottjer, D.J., Berelson, W.M., Bergquist, B.A., and Corsetti, F.A., 2016, Mercury anomalies and the timing of biotic recovery following the end-Triassic mass extinction: Nature Communications, v. 7, https://doi.org/10.1038/ncomms11147.

Wang, Q.F., and Groves, D., 2018, Carlin-style gold deposits, Youjiang Basin, China: Tectono-thermal and structural analogues of the Carlin-type gold deposits, Nevada, USA: Mineralium Deposita, v. 53, p. 909–918, https://doi.org/10.1007/s00126-018-0837-x.

Wei, S.D., Liu, H., and Zhao, J.H., 2018, Tectonic evolution of the western Jiangnan Orogen: Constraints from the Neoproterozoic igneous rocks in the Fanjingshan region, South China: Precambrian Research, v. 318, p. 89–102, https://doi.org/10.1016/j.precamres.2018.10.006.

Wilkinson, J.J., 2013, Triggers for the formation of porphyry ore deposits in magmatic arcs: Nature Geoscience, v. 6, p. 917–925, https://doi.org/10.1038/ngeo1940.

Wu, Y.F., Evans, K., Li, J.W., Fougerouse, D., Large, R.R., and Guagliardo, P., 2019, Metal remobilization and ore-fluid perturbation during episodic replacement of auriferous pyrite from an epizonal orogenic gold deposit: Geochimica et Cosmochimica Acta, v. 245, p. 98–117, https://doi.org/10.1016/j.gca.2018.10.031.

Xie, Z.J., Xia, Y., Cline, J., Pribil, M.J., Koenig, A.E., Tan, Q.P., Wei, D.T., Wang, Z.P., and Yan, J., 2018a, Magmatic origin for sediment-Hosted Au deposits, Guizhou province, China: In situ chemistry and sulfur isotope composition of pyrites, Shuiyindong and Jinfeng deposits: Economic Geology, v. 113, p. 1627–1652, https://doi.org/10.5382/econgeo.2018.4607.

Xie, Z.J., Xia, Y., Cline, J.S., Koenig, A., Wei, D.T., Tan, Q.P., and Wang, Z.P., 2018b, Are there Carlin-type gold deposits in China?: A comparison of the Guizhou, China, deposits with Nevada, USA, deposits, *in* Muntean, J.L., ed., Diversity of Carlin-Style Gold Deposits: Reviews in Economic Geology, Society of Economic Geologists, v. 20, p. 187–233, https://doi.org/10.5382/rev.20.06.

Yan, J., Hu, R.Z., Liu, S., Lin, Y.T., Zhang, J.C., and Fu, S.L., 2018, Nano-SIMS element mapping and sulfur isotope analysis of Au-bearing pyrite from Lannigou Carlin-type Au deposit in SW China: New insights into the origin and evolution of Au-bearing fluids: Ore Geology Reviews, v. 92, p. 29–41, https://doi.org/10.1016/j.oregeorev.2017.10.015.

Yao, J.L., Cawood, P.A., Shu, L.S., and Zhao, G.C., 2019, Jiangnan Orogen, South China: A ~970–820 Ma Rodinia margin accretionary belt: Earth-Science Reviews, v. 196, no. 102872, https://doi.org/10.1016/j.earscirev.2019.05.016.

Yin, R.S., Feng, X.B., and Meng, B., 2013, Stable mercury isotope variation in rice plants (Oryza sativa L.) from the Wanshan mercury mining district, SW China: Environmental Science & Technology, v. 47, p. 2238–2245, https://doi.org/10.1021/es304302a.

Yin, R.S., Feng, X.B., Chen, B., Zhang, J., Wang, W., and Li, X., 2015, Identifying the sources and processes of mercury in subtropical estuarine and ocean sediments using Hg isotopic composition: Environmental Science & Technology, v. 49, p. 1347–1355, https://doi.org/10.1021/es504070y.

Yin, R.S., Krabbenhoft, D.P., Bergquist, B.A., Zheng, W., Lepak, R.F., and Hurley, J.P., 2016, Effects of mercury and thallium concentrations on high precision determination of mercury isotopic composition by Neptune Plus multiple collector inductively coupled plasma mass spectrometry: Journal of Analytical Atomic Spectrometry, v. 31, p. 2060–2068, https://doi.org/10.1039/C6JA00107F.

Yin, R.S., Xu, L.G., Lehmann, B., Lepak, R.F., Hurley, J.P., Mao, J.W., Feng, X.B., and Hu, R.Z., 2017, Anomalous mercury enrichment in Early Cambrian black shales of South China: Mercury isotopes indicate a seawater source: Chemical Geology, v. 467, p. 159–167, https://doi.org/10.1016/j.chemgeo.2017.08.010.

Yin, R.S., Deng, C.Z., Lehmann, B., Sun, G.Y., Lepak, R.F., Hurley, J.P., Zhao, C.H., Xu, G.W., Tan, Q.P., Xie, G.Z., and Hu, R.Z., 2019, Magmatic-hydrothermal origin of mercury in Carlin-style and epithermal gold deposits in China: Evidence from mercury stable isotopes: ACS Earth and Space Chemistry, v. 3, p. 1631–1639, https://doi.org/10.1021/acsearthspacechem.9b00111.

Yin, R.S., Chen, D., Pan, X., Deng, C.Z., Chen, L.M., Song, X.Y., Yu, S.Y., Zhu, C.W., Wei, X., Xu, Y., Feng, X.B., Blum, J.D., and Lehmann, B., 2022, Mantle Hg isotopic heterogeneity and evidence of oceanic Hg recycling into the mantle: Nature Communications, v. 13, no. 948, https://doi.org/10.1038/s41467-022-28577-1.

Zerkle, A.L., Yin, R.S., Chen, C.Y., Li, X.D., Izon, G.J., and Grasby, S.E., 2020, Anomalous fractionation of mercury isotopes in the Late Archean atmosphere: Nature Communications, v. 11, 1709, https://doi.org/10.1038/s41467-020-15495-3.

Zhao, G.C., and Cawood, P.A., 2012, Precambrian geology of China: Precambrian Research, v. 222–223, p. 13–54, https://doi.org/10.1016/j.precamres.2012.09.017.

Zhu, J., Zhang, Z.C., Santosh, M., and Jin, Z.L., 2020, Carlin-style gold province linked to the extinct E'meishan plume: Earth and Planetary Science Letters, v. 530, https://doi.org/10.1016/j.epsl.2019.115940.

Zhu, J.J., Zhong, H., Xie, G.Q., Zhao, C.H., Xu, L.L., and Lu, G., 2016, Origin and geological implication of the inherited zircon from felsic dykes, Youjiang basin, China [in Chinese with English abstract]: Acta Petrological Sinica, v. 32, p. 3269–3280.

Science Editor: Mihai Ducea
Associate Editor: Ryan Mathur

Manuscript Received 12 June 2022
Revised Manuscript Received 11 October 2022
Manuscript Accepted 4 December 2022

Printed in the USA